May 2023

A Light Gradient Boosting Machine-enabled Model to Predict Radiation-induced Toxicities in Cancer Patients Receiving Chemoradiotherapy

Zirui Jiang

A LIGHT GRADIENT BOOSTING MACHINE-ENABLED MODEL TO PREDICT RADIATION-INDUCED TOXICITIES IN CANCER PATIENTS RECEIVING CHEMORADIOTHERAPY

By

Zirui Jiang

Bachelor of Science – Electrical Engineering
Bachelor of Science – Physics
University of Wisconsin Madison
2019

A thesis submitted in partial fulfillment
of the requirements for the

Master of Science – Health Physics

Department of Health Physics and Diagnostic Sciences
School of Integrated Health Science
The Graduate College

University of Nevada, Las Vegas
May 2023

UNLV | GRADUATE COLLEGE

Thesis Approval

The Graduate College
The University of Nevada, Las Vegas

April 10, 2023

This thesis prepared by

Zirui Jiang

entitled

A Light Gradient Boosting Machine-enabled Model to Predict Radiation-induced Toxicities in Cancer Patients Receiving Chemoradiotherapy

is approved in partial fulfillment of the requirements for the degree of

Master of Science – Health Physics
Department of Health Physics and Diagnostic Sciences

Yu Kuang, Ph.D.
Examination Committee Chair

Steen Madsen, Ph.D.
Examination Committee Member

Zaijing Sun, Ph.D.
Examination Committee Member

Shengjie Zhai, Ph.D.
Graduate College Faculty Representative

Alyssa Crittenden, Ph.D.
Vice Provost for Graduate Education & Dean of the Graduate College

Abstract

The objective of this study was to develop a predictive model that utilizes a Light Gradient Boosting Machine (Light-GBM) to accurately assess the risk of severe radiation-induced toxicities in cancer patients undergoing chemoradiotherapy. The occurrence of these toxicities can have a substantial impact on the patients' quality of life. The Light-GBM model using clinical feature alone or integrating radiomic features extracted from computed tomography (CT) images used in treatment planning with clinical features can enhance the accuracy of early prediction.

The study included 179 breast cancer patients and 223 patients with nasopharynx cancer who were treated with both radiotherapy and chemotherapy from April 2005 to October 2020. All of the patients with nasopharynx cancer had pre/postoperative CT/MR scans. The clinical features extracted from the medical records of patients included age, cancer stage, tumor size, tumor location, medical history, chemotherapy drugs, targeted therapy drugs, hormone therapy drugs, distant metastases, surgery, radiation therapy position, radiotherapy dose. The additional clinical features were also extracted from breast cancer patients, including electrocardiograph (ECG) signal score, and left ventricular ejection fraction (LVEF) value before radiotherapy. The Light-GBM was used to develop predictive models to predict oral mucositis and radiation dermatitis in nasopharynx patients and cardiotoxicity in breast cancer patients, respectively. The utility of the developed models was evaluated via receiver operating characteristic curve (ROC) and area under the curve (AUC).

In breast cancer case, the patients were randomly divided into a training set (n=150) and a test set (n=29). A Light GBM enabled predictive model was developed using patients’ clinical features. The utility of the developed model was evaluated via ROC. The AUC of the

cardiotoxicity Light-GBM model was 0.82, higher than the clinical significance threshold of 0.7. Age, LVEF value before radiotherapy, cancer position, targeted therapy, tumor stage, and hormone therapy were the most valuable influencing factors. Specifically, we found that more severe cardiotoxicity occurred in patients with older age, higher LVEF value before radiotherapy, later tumor stage, and abnormal ECG signals with bradycardia, tachycardia, T wave, and Q wave abnormalities.

For nasopharyngeal cancer patients, we developed two Light-GBM machine learning models: Model A, which included only clinical features, and Model B, which combined radiomic and clinical features. The models were trained using a training set of 200 samples and validated with a test set of 20 samples. A total of 756 radiomic features were extracted from the planning target volume (PTV), gross tumor volume (GTV), clinical target volume-GTV (CTV-GTV), clinical target volume (CTV), and organs at risk regions in the images. The models' abilities to predict severe toxicities were evaluated using ROC analysis in the validation cohort.

The AUC values for Model A, which predicted six different toxicities (radiation oral mucositis, radiation dermatitis, skin ulcer, sternocleidomastoid muscle toxicity, thyroid toxicity, and skin thickness toxicity), were 0.8, 0.71, 0.72, 0.68, 0.75, and 0.64, respectively. In contrast, Model B demonstrated increased AUC values of 0.86, 0.81, 0.84, 0.77, 0.89, and 0.8. Feature importance analysis revealed that T stage, age, radiation dose, chemotherapy drugs, and 14 radiomic features were the most valuable risk prediction factors.

The results of this study illustrate the potential of utilizing machine learning models to predict various radiation-related toxicities. This approach facilitates the early identification of patients who may benefit from personalized chemoradiotherapy, timely interventions during or after chemoradiotherapy, or the use of alternative treatment technologies.

Acknowledgements

I would like to express my sincere gratitude to the professors and mentors at the University of Nevada, Las Vegas who have been instrumental in guiding me throughout my graduate studies. Firstly, I extend my heartfelt appreciation to my committee chair and research advisor, Dr. Yu Kuang. Throughout my two-year master's program, Dr. Kuang has been a patient and dedicated guide, mentoring me from a novice learner to a first author and near-completer of my master's degree. His meticulous and detailed instruction in the fields of medical physics, artificial intelligence, and radiation toxicity has been invaluable to me, and I am deeply thankful for his guidance.

In addition, I extend my thanks to my committee members, Dr. Steen Madsen, Dr. Shengjie Zhai, and Dr. Zaijing Sun, for providing me with necessary counsel and guidance, which has significantly contributed to my growth and development as a researcher. Furthermore, I would like to give special recognition to Dr. Yin Liang from Sichuan Cancer Hospital, China, for his invaluable assistance with data collection and support.

Overall, I am deeply grateful to all these individuals for their unwavering support and guidance, which has enabled me to achieve my academic goals and prepared me for my future endeavors.

Table of Contents

List of Tables

List of Figures

Chapter 1 Introduction

1.1 Radiation Therapy and Radiation-included Toxicity

Radiation therapy (RT) is a widely accepted treatment option for cancerous tumors. Although administering RT optimally requires striking a balance between maximizing the dose to the tumor while minimizing the dose to normal tissue, the mechanism of radiation-induced cell death does not solely target cancer cells [1]. RT employs ionizing radiation to eliminate tumor tissue, but it can also harm normal tissue by causing direct or indirect damage to DNA through ionizing radiation. This triggers a sequence of events that may lead to cell death and toxicity [2].

The toxic effects of RT are divided into three categories: early, subacute, and late [3]. Early toxicities typically occur during cancer treatment or immediately after its completion. Early toxicities may appear within hours or days of receiving therapy, and they are generally temporary, resolving as the body recovers from treatment. Examples of early toxicities include acute nausea and vomiting, immediate skin reactions, or allergic reactions to chemotherapy drugs. Subacute toxicities manifest within days to a few weeks after the initiation of treatment and may persist for some time following its completion [4]. Subacute toxicities can be a continuation of early toxicities or new symptoms that develop as the cumulative effect of treatment takes its toll on the body. Examples of subacute toxicities include fatigue, mucositis, and hematological toxicity. Late toxicities, also known as long-term side effects or late effects, are complications that arise months or even years after cancer treatment has been completed [3]. Unlike early and subacute toxicities, late toxicities can have a more chronic or long-lasting impact on a patient's health and quality of life. Some common late toxicities include secondary

cancers, cardiovascular issues, lung problems, kidney damage, neurological issues, hormonal imbalances, bone issues, and growth and development issues [3, 4]. How to manage and when to intervene those toxicities in cancer patients receiving chemoradiotherapy is a focus of clinical attention.

1.2 Cardiotoxicity in Breast Cancer Patients Receiving Radiotherapy

Radiation therapy, in particular, has played a vital role in breast cancer treatment, which is the most common cancer type among women globally [5, 6]. According to the American Cancer Society's biennial report on breast cancer statistics in the United States, the death rate for breast cancer was 1.3% between 2011 and 2017 [7].Fortunately, the prognosis for operable non-metastatic breast cancer is excellent, with an estimated 5-year overall survival rate of 90%. Currently, radiation therapy is a standard of care for managing this type of breast cancer as it has been shown to reduce breast cancer mortality [8].

However, RT can have negative effects on cardiovascular health of breast cancer patients, which can significantly impact patients' survival and quality of life [9]. Its associated cardiotoxicity can lead to cardiomyopathy, and in severe cases, progress to heart failure, hindering the effectiveness of RT [10]. Currently, the risk of potential cardiotoxicity remains a concern. An accurate method of evaluating cardiac radiation exposure can predict radiation-induced cardiac side effects, and this information can be used to adjust the clinical treatment plan.

1.3 Radiation-induced Toxicities in Nasopharynx Patients Undergoing Concurrent Chemoradiation Therapy

Nasopharynx cancer (NPC) is a type of cell carcinoma that originates from the inner lining of the nasopharynx and has a tendency to spread to other parts of the body. Its aggressive nature is one of the biggest obstacles in treating NPC, with a very poor outcome once it has metastasized, resulting in a 91% death rate within a year after the initial metastasis [9]. NPC is known for its early spread to the lymphatic system and a high likelihood of spreading through the bloodstream. Many patients are diagnosed at an advanced stage of the disease, which makes treatment challenging due to the nasopharynx's proximity to vital structures [10].

Nasopharyngeal cancer is associated with various factors, including genetic, dietary, environmental, and EB virus infections [14]. Due to the nasopharynx's hidden location, early symptoms of nasopharyngeal cancer are complex and lack distinct characteristics, which makes it difficult for patients to discover the disease on their own and easy for it to be overlooked. Even when patients seek medical attention, 80% of cases are already in the late stage.

There are several treatment options available for nasopharyngeal cancer, including radiation therapy, surgical treatment, and immunotherapy. However, more than 95% of nasopharyngeal cancer cases belong to poorly differentiated or undifferentiated types with high malignancy and rapid growth, often leading to lymph node or vascular metastasis. Unfortunately, at the time of diagnosis, 75% of patients have already reached stages III and IV, making surgical treatment unsuitable for patients in these stages as it has a high risk of recurrence or metastasis [12, 15, 16]. Therefore, radiation therapy is considered the first-line treatment for nasopharyngeal cancer.

Radiation therapy can inadvertently damage the muscle fibers or surrounding blood vessels, leading to inflammation, scarring, or muscle atrophy. Common toxicities experienced by nasopharyngeal cancer patients undergoing chemoradiotherapy include radiation-induced oral mucositis, dermatitis, skin ulcers, muscle damage in the sternocleidomastoid, thyroid dysfunction, and increased skin thickness [7-10].

Severe toxicities can substantially reduce patients' quality of life. For example, oral mucositis may cause difficulty swallowing, leading to malnutrition and weight loss. Radiation dermatitis and skin ulcers can be painful and limit patients' daily activities. Thyroid dysfunction can affect energy levels, metabolism, and overall well-being. Addressing these toxicities can help improve patients' quality of life during and after cancer treatment [7-10].

1.4 DICOM-RT

In the nasopharynx cancer toxicity study, a predict model was built via combing patients' clinical data and radiomic features to improve prediction performance. The DICOM standard, widely used in radiology for diagnostic imaging, has been extended for use in sub-specialties such as radiation therapy through the development of DICOM-RT (DICOM in Radiation Therapy) [11]. In our study, patients were scanned using a CT scanner, which produced DICOM computed tomography (CT) images that were used for the Light-GBM model building. DICOM files can be complex as it is essential to have a thorough understanding of the standard and appropriate tools for data analysis. Additionally, patient privacy and data security are vital considerations when working with medical imaging data.

1.5 Imaging Biomarker Explorer

The Imaging Biomarker Explorer (IBEX) is a radiomics tool that is freely available to the public [12]. It was developed by the MD Anderson Cancer Center with a user-friendly interface to facilitate the extraction and calculation of quantitative features from medical images, which can assist in cancer treatment decision-making. For this study, IBEX was used to extract various types of features commonly used in radiomics for medical physics. These features were classified into groups, such as gray level co-occurrence matrix, gray level run length matrix, intensity, neighborhood intensity difference matrix, and shape. Users can modify the parameters for each feature set as required. The use of IBEX allowed us to extract critical data from medical images, which could aid in the development of cancer treatment plans. The tool's accessibility and user-friendly interface make it a valuable resource for healthcare professionals and researchers [13-16]. Figure 1 shows the IBEX user interface for extracting features from patient’s DICOM-RT files.

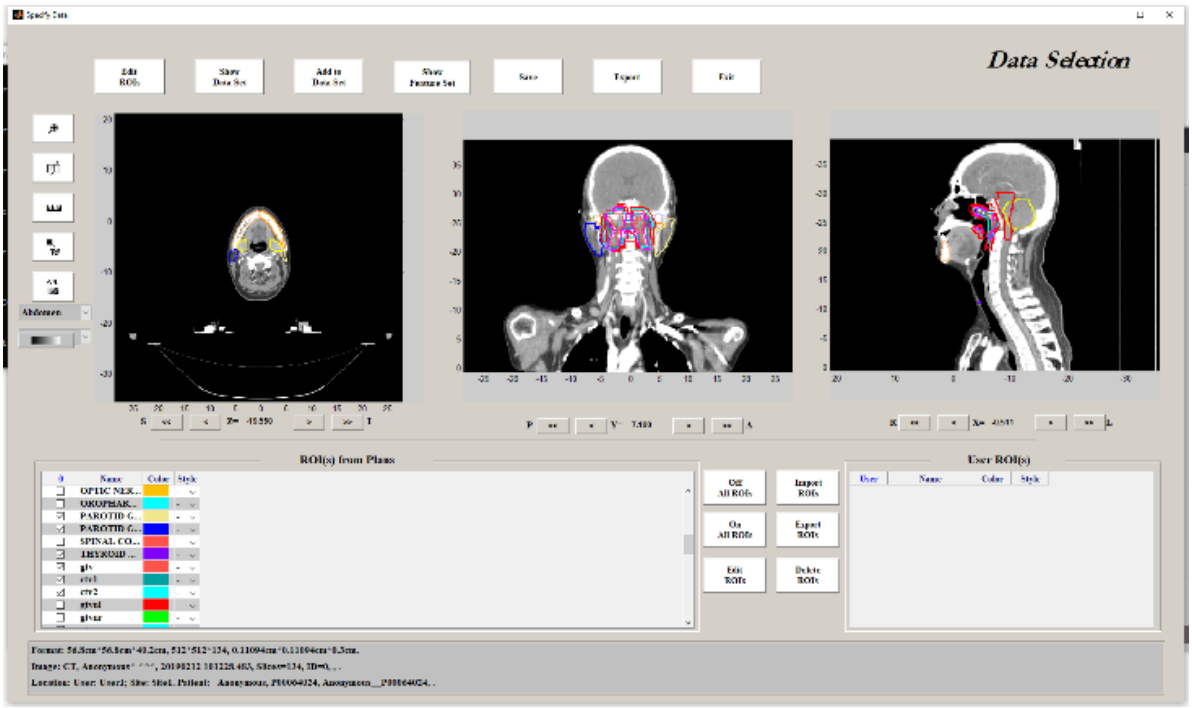

Figure 1: Example showing IBEX user interface for extracting features from patient's DICOM-RT files

1.6 Light Gradient Boosting Machine (Light-GBM) Model

The Light-GBM Model [17-19] is a gradient boosting framework that uses tree-based learning algorithms. It has been optimized for efficiency and distribution, offering several key benefits, such as faster training speed, improved performance, lower memory consumption, higher precision, support for parallel and distributed learning, GPU compatibility, and the ability to process large-scale data. Contrary to most decision tree learning algorithms, which construct trees level-wise, Light-GBM grows trees leaf-wise (best-first) [20] (as shown in Figures 2 and 3). This algorithm selects the leaf with the highest delta loss for expansion, keeping the leaves fixed to achieve lower loss than level-wise algorithms. Light-GBM uses histogram-based algorithms to place continuous feature values into discrete bins. [19, 21, 22]. This approach accelerates the

training process, reduces memory usage, and offers several benefits, including lower computational cost for calculating the gain of each split, histogram subtraction for additional speed, lower memory consumption, and reduced communication cost for distributed learning.

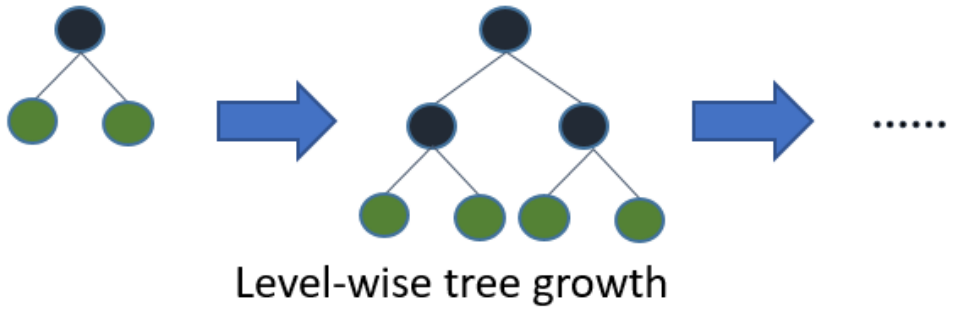

Figure 2: Normal decision tree learning algorithms.

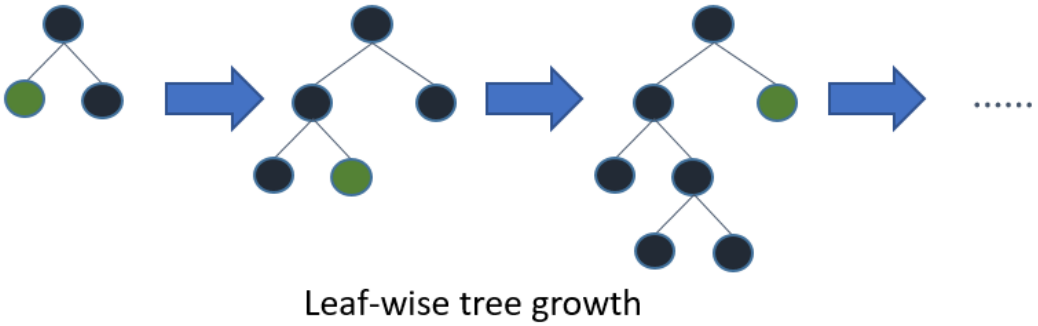

Figure 3: Light-GBM decision tree learning algorithms.

Owing to the leaf-wise tree growth characteristic, Light-GBM may cause overfitting with small datasets. To address this problem, it includes the parameter "max_depth" to limit tree depth. However, even with "max_depth" set, Light-GBM continues to grow tree leaf-wise.

Light-GBM offers a unique approach to handling categorical features during the splitting process. While one-hot encoding is a widely used method for representing categorical features, it may not be the most efficient approach for tree-based models, especially for high-cardinality categorical features. When a tree is built on one-hot encoded features, it may become imbalanced and require a deep structure to achieve high accuracy. Instead of using one-hot encoding, Light-GBM uses a technique that groups the categories of a categorical feature into two sets. For a feature with k categories, there are 2^(k-1) - 1 possible partitions. However, Light-GBM has an efficient solution for finding the optimal partition that takes approximately (k * log(k)) time for regression trees [22].

Light-GBM has seen success in many medical applications. For instance, Gao et al. developed a model to predict acute kidney injury in ICU patients using Light-GBM [23]. Zhou et al. showed that Light-GBM outperforms Support Vector Machine (SVM) in detecting Alzheimer's disease from brain imaging samples [17]. By using Light-GBM as an auxiliary decision support tool, clinical medical staff can work more efficiently by leveraging data-driven insights, ultimately reducing workload. This complementary relationship between Light-GBM and clinical medical staff helps improve diagnosis and treatment outcomes [18].

In this project, a Light-GBM-enabled predictive model was developed to integrate patients' electronic medical records (EMRs) to predict patients' toxicities years after undergoing chemoradiotherapy. By leveraging the power of Light-GBM, the predictive model offers improved accuracy and efficiency in forecasting treatment induced toxicities, ultimately contributing to better patient care and management strategies. With Light-GBM's continued advancement and application in medical scenarios, we can expect to see more innovations that help healthcare professionals make data-driven decisions to improve patient care.

1.7 Receiver Operating Characteristic Curves and Area Under the Curve value

Receiver Operating Characteristic (ROC) curves and Area Under the Curve **(**AUC) are commonly used in machine learning for various purposes, such as evaluating the performance of diagnostic, decision support, and prognostic models. These curves have been thoroughly researched and applied in various statistical and medical domains [24-26].

The ROC curve serves as a graphical representation that delineates a classifier's performance across a range of classification thresholds. By plotting the True Positive Rate (TPR, also known as sensitivity) against the False Positive Rate (FPR, or 1-specificity), the ROC curve demonstrates the model's capacity to accurately classify instances while concurrently minimizing erroneous classifications (shown in Figure 4 below). In contrast, the Area Under the Curve (AUC) quantifies a classifier's overall performance as a single value, derived from calculating the area beneath the ROC curve. AUC values range from 0 to 1, with values exceeding 0.5 signifying a classifier possessing some level of discriminatory ability—higher values are indicative of enhanced performance. A classifier with an AUC of 1 demonstrates perfect discrimination between positive and negative classes.

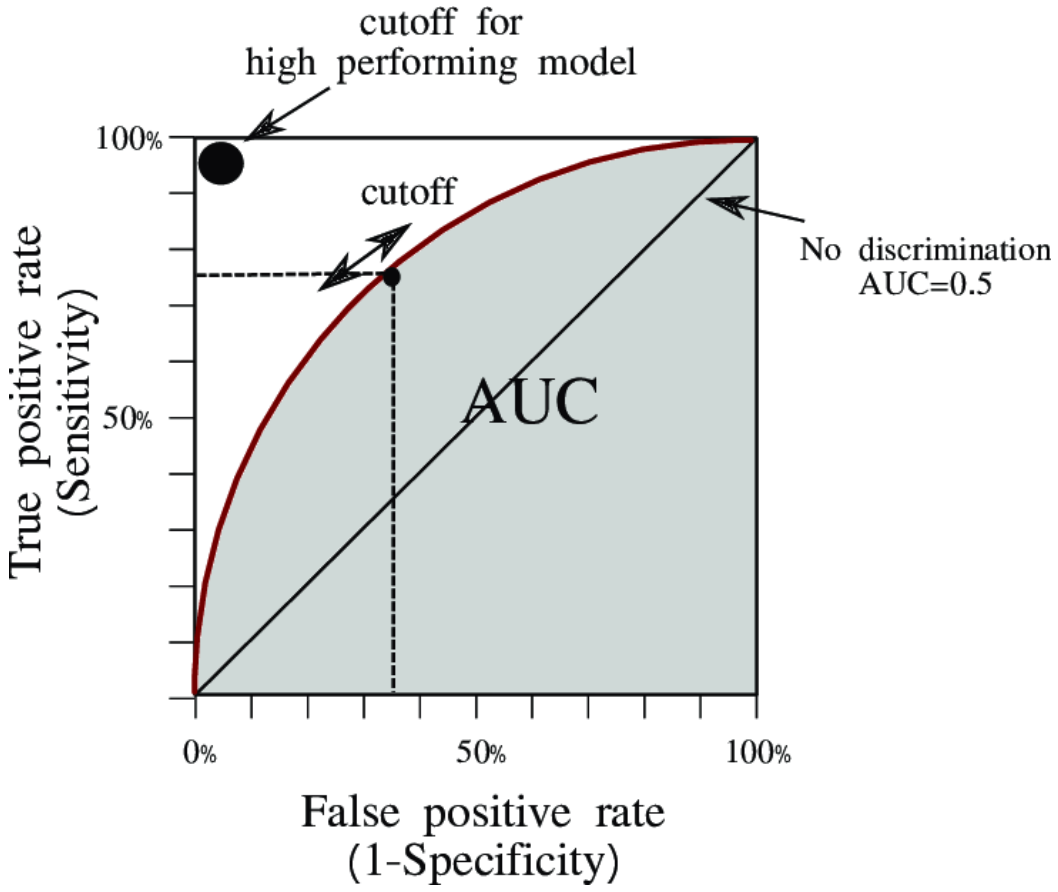

Figure 4: the ROC curve by plotting the TPR against FPR.

Binary tests are a popular classification method used in medicine. They generate two clear-cut outcomes (e.g. positive or negative) to establish the unknown, such as determining the presence or absence of toxicity. The precision of these tests is often analyzed by using sensitivity (SN) and specificity (SP) as measurement tools, where:

$$SN = \frac{TP}{TP+FN} \quad (1)$$

$$SP = \frac{TN}{TN+FP} \quad (2)$$

In the context of binary classification, true positives (TP), true negatives (TN), false positives (FP), and false negatives (FN) are terms used to describe the outcomes of a classification algorithm. True Positives (TP): These are cases where the model correctly predicts the positive class. True Negatives (TN): These are cases where the model correctly predicts the negative class. False Positives (FP): These are cases where the model incorrectly predicts the positive class. False Negatives (FN): These are cases where the model incorrectly predicts the negative class.

1.8 Objectives

The goal of this study is to investigate the feasibility of utilizing Light-GBM for predicting cardiotoxicity in breast cancer patients undergoing radiotherapy and for predicting radiation-induced toxicities in nasopharynx cancer patients undergoing concurrent chemoradiation therapy, respectively. The models used patients' chart data extracted from EMRs to predict potential cardiotoxicity and used combined radiomic features extracted from patients' CT data and clinical features extracted from EMRs to predict the nasopharynx cancer toxicity in the years following chemoradiotherapy treatment. This will facilitate timely intervention and appropriate treatment in patients with both breast cancer and nasopharynx cancer. These models serve as a robust, quantitative, and predictive diagnostic tool for radiotherapy-induced toxicities, providing clinically actionable information to the clinical end-users, such as radiation oncologists, for reliable prediction of several toxicities.

Chapter 2 Development and validation of a light-GBM enabled model to predict cardiotoxicity in breast cancer patients receiving radiotherapy

2.1 Introduction

2.1.1 RT-induced Cardiotoxicity in Breast Cancer Patients

Radiotherapy is an effective treatment in reducing the risk of local recurrence, shrinking tumor size, and decreasing mortality rates in breast cancer patients [27]. However, it can also adversely affect normal tissues within the irradiation field, particularly the heart. These toxicities caused by radiation can significantly decrease the quality of life for cancer survivors.

Radiation therapy for breast cancer may result in long-term cardiac toxicity, such as heart failure, coronary artery disease, myocardial infarction, and cardiovascular death, up to 10 years post-treatment. The risks associated with these toxicities are estimated to range from 1.2 to 3.5 times for patients who received left breast treatment, which entails higher heart exposure, versus those treated for the right breast or not exposed to RT at all [28-31].

Retrospective studies analyzing the medical records of breast cancer patients who received radiation therapy and underwent coronary angiography several years later have established a correlation between radiation exposure and the location of stenosis. These studies discovered that stenosis commonly occurred in the left anterior descending artery [32, 33]. Previous studies have emphasized the importance of considering both the location of radiation doses on heart structures and their localized effects, particularly on coronary arteries [34-36].

2.1.2 Left Ventricular Ejection Fraction

Current methods for identifying early stages of chemoradiotherapy-induced cardiotoxicity remain suboptimal and costly. The most commonly employed technique for monitoring anthracycline-induced cardiotoxicity is cardiac magnetic resonance imaging (CMR), which offer a comprehensive assessment for detecting cancer therapy-related cardiac dysfunction (CTRCD) [37, 38]. In recent years, cardiac ultrasound has been adopted in oncology for detecting cardiotoxic treatment-induced changes in Left Ventricular Ejection Fraction (LVEF). This approach utilizes real-time imaging, noninvasive nature, non-ionizing radiation, and lower cost ultrasound imaging systems, and has proven useful in the early diagnosis of chemoradiotherapy-induced cardiotoxicity [39].

LVEF is a critical indicator of left ventricular systolic function, measured as the ratio of blood expelled from the left ventricle during systole (stroke volume) to the volume of blood in the ventricle at the end of diastole (end-diastolic volume). Stroke volume is calculated as the difference between end-diastolic volume (EDV) and end-systolic volume (ESV). The formula for LVEF is as follows: LVEF = (SV/EDV) x 100. The SV and EDV values can be measured using cardiac ultrasound.

The American College of Cardiology (ACC) has established a simple classification system for the clinical use of LVEF, which includes the following categories: Hyperdynamic (LVEF > 70%), normal (LVEF between 50% and 70% with a midpoint of 60%), mild dysfunction (LVEF between 40% and 49% with a midpoint of 45%), moderate dysfunction (LVEF between 30% and 39% with a midpoint of 35%), and severe dysfunction (LVEF < 30%) [36]. According to the American Society of Echocardiography (ASE) and the European Association of Cardiovascular Imaging (EACVI), cardiotoxicity is defined as a decline in Left

Ventricular Ejection Fraction (LVEF) by more than 10% below the lower threshold of normal, which is set at 53%, and is not related to any symptoms [40].

Echocardiography has been employed in recent years to elucidate early RT-induced cardiovascular effects in chemotherapy patients [41, 42]. The New York Heart Association (NYHA) classifies a decrease greater than 15% in the global longitudinal strain (GLS) from the baseline GLS value as evidence of subclinical left ventricular (LV) dysfunction [43, 44]. In this study, two-dimensional echocardiography with speckle-tracking imaging was conducted at baseline (pre-chemotherapy), before and after radiation therapy (pre-RT and post-RT), and 6 months post-RT, used together with LVEF to enhance accuracy.

2.1.3 Objective of the Work

Previous research on cardiotoxicity has primarily focused on anthracycline chemotherapy drugs [45-48], trastuzumab [42, 49, 50], and standalone radiotherapy [51]. However, cardiotoxicity generally stems from the combined effects of multiple treatments rather than an individual factor. Tuohinen et al. [13] utilized ECG and echocardiography to assess chemoradiotherapy toxicity without developing a predictive model. Ryberg et al [41] identified risk factors for cardiotoxicity, using factors including targeted therapy, advanced tumor stage, age, anthracyclines, targeted drugs, and abnormal ECG signals before therapy. In this work, we develop an innovative model for predicting cardiotoxicity arising from chemoradiotherapy using a combination of echocardiography and ECG for toxicity assessment. We further considered atypical LVEF values as a potential feature associated with an increased risk of cardiotoxicity.

2.2 Methods and Materials

2.2.1 Patients and Inclusion Criteria

A total of 179 breast cancer patients were included in this study with stage I-IV breast cancer who underwent both radiation therapy and chemotherapy at Sichuan Cancer Hospital, China, between April 2005 and October 2020. The patients were followed for one to four years after receiving therapy. Patients with the majority of their data missing were excluded from the study. For patients missing one or two characteristics, since “N/A” constituted only a small percentage of the total data for each patient (0.56% to 4.47%), we replaced “N/A” with the median value of this feature for all patients. To achieve more accurate cardiotoxicity results from ultrasound LVEF values and ECG scores, a cardiologist and a sonographer provided their expertise and assistance.

2.2.2 Flowchart of Light-GBM Model

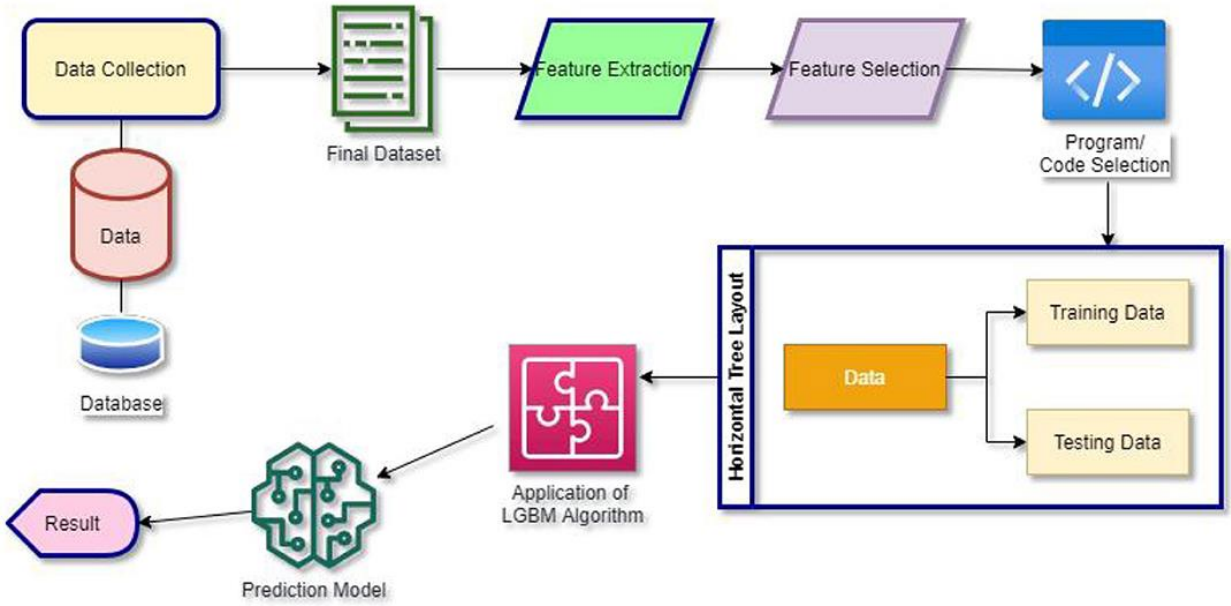

Figure 5: Flowchart of the development of a Light-GBM predictive model.

Figure 5 illustrates the workflow for the Light-GBM model applied to breast cancer patients for cardiotoxicity prediction. After data collection, features that failed to meet the specified criteria were removed and those meeting the inclusion criteria were retained. The selected features were then preprocessed and normalized to numerical values (Section 2.2.2) for the Light-GBM model's interpretation. Subsequently, the dataset was randomly partitioned into a training set (n=150) and a test set (n=29), with the training set used for model development and the test set employed for performance evaluation.

Then, we proceeded to train the Light-GBM model, adjusting various hyperparameters, such as learning rate, maximum tree depth, and the number of boosting rounds, to guarantee optimal model development. The final specific configurations were established as follows: the

number of leaves at 31, the learning rate at 0.05, "feature_fraction" at 0.9, "bagging_fraction" at 0.8, and "bagging_freq" at 5, wherein every 5th iteration was utilized for bagging. The trained model was saved to a file named 'model.txt' using the save_model() function. Subsequently, the trained model were employed to make predictions on the test dataset using the predict() function. Concurrently, the model's performance was evaluated using a 10-fold cross-validation method, which aimed to estimate generalization capabilities and avert overfitting. This procedure was conducted ten times with distinct randomly selected training and test datasets.

In the final step, the prediction outcomes from each iteration in the 10-fold cross-validation were examined via deriving performance metrics, encompassing ROC, AUC, accuracy, precision, recall, F1-score, and others.

2.2.2 Features and Feature Normalization

All features used for model training are listed in Table 1 below.

Table1. Training factors for Light-GBM Model

Variable		Number	Percentage
Gender	Male	1	0.56%
	Female	178	99.44%
Age	<40	17	9.50%
	40~60	128	71.51%
	>60	29	16.20%
Tumor size	T1	39	21.79%
	T2	113	63.13%
	T3	11	6.15%
	T4	8	4.47%
	N/A	8	4.47%
Cancer position	Right	94	52.51%
	Left	85	47.49%
Cancer stage	I	19	10.61%
	II	90	50.28%
	III	54	30.17%
	IV	16	8.94%
Heart disease history	Yes	54	30.17%
	No	119	66.48%
	N/A	6	3.35%
ECG signal score before radiotherapy	Normal	119	66.48%
	Arrhythmia, premature atria, and premature ventricular beats	12	6.70%
	Bradycardia and tachycardia	15	8.38%
	T wave and Q wave abnormalities, intra--atrialblock, and ST segment upper oblique elevation	26	14.53%
	N/A	7	3.91%
Distant metastases	Yes	33	18.44%
	No	145	81.01%
	N/A	1	0.56%
Hormone therapy	Yes	110	61.45%
	No	66	36.87%
	N/A	2	1.12%
chemotherapy drugs	Epicorubicin and doxorubicin	155	86.59%
	Cyclophosphamide, paclitaxel, and docetaxel	19	10.61%
	Capecitabine, vinorelbine, gemcitabine, cisplatin, nedaplatin, carboplatin, xeloda	3	1.68%
radiotherapy dose	<40Gy	21	11.73%
	40~50GY	142	79.33%
	>50GY	16	8.94%
surgery	Breast conserving	116	64.80%
	Total excision	63	35.20%

targeted therapy drugs	None	115	64.25%
	Trastuzumab	41	22.91%
	Pertuzumab	22	12.29%
	Bevacizumab	1	0.56%
LVEF value before radiotherapy	<60	15	8.38%
	60~70	113	63.13%
	>70	51	28.49%

To optimize the machine learning model's performance, all features were normalized, and certain categorical features were transformed into binary values. "Yes or no" questions were encoded as 1 for "yes" and 0 for "no," which allowed for effective model training and improved efficiency, such as heart disease history, distant metastases, hormone therapy, and target therapy drugs.

For categorical features with only two options (e.g., gender, cancer position, and surgery), we encoded male, left, and breast-conserving as 0 and female, right, and total excision as 1. For numerical features (e.g., age, radiotherapy dose, and LVEF value before radiation therapy), we divided the values by 100 to fit the required range. For cancer stage and tumor size, which have multiple categories, we assigned T1 and stage 1 a value of 0, T2 a value of 0.33, T3 a value of 0.66, and T4 a value of 1. Finally, we included the ECG signal scores before radiotherapy, chemotherapy drugs, and target therapy drugs as additional features in the model. Based on clinical experience and literatures, we defined a normal ECG signal as 0 and various types of arrhythmias, premature atrial and ventricular beats, bradycardia, and tachycardia as 0.1. T wave and Q wave abnormalities, intra-atrial block, and ST segment elevation were assigned a value of 0.3. In terms of the potential cardiotoxicity of chemotherapy drugs and target therapy drugs, we rated epirubicin and doxorubicin as 0.3 (high potential for cardiotoxicity), cyclophosphamide, paclitaxel, and docetaxel as 0.2 (moderate potential for cardiotoxicity), and

capecitabine, vinorelbine, gemcitabine, cisplatin, nedaplatin, carboplatin, and xeloda as 0.1 (low potential for cardiotoxicity). Similarly, we rated bevacizumab as 0.3, pertuzumab as 0.2, and pertuzumab as 0.1 based on their potential for cardiotoxicity. All optimized feature values are consolidated in Excel CSV files to facilitate seamless integration with the Light-GBM model.

2.2.3 Model Building

The Light-GBM library is implemented as a standalone module, and model development is carried out using the scikit-learn API. Python is employed to create training and validation datasets for processing patient CSV files in this project. Initially, we import LightGBM, pandas, and mean_squared_error from the sklearn library. Subsequently, the training and test datasets are read from CSV files and partitioned into features (X_train and X_test) and target variables (y_train and y_test). The pandas DataFrames are then transformed into LightGBM Datasets (lgb_train and lgb_eval) to facilitate model training.

Following this, we establish the model's initial hyperparameters: number of leaves (n=35), learning rate (0.07), "feature_fraction" (0.09), and "bagging_fraction" (0.8). The LightGBM model is trained using the lgb.train() function with the specified parameters, setting the number of boosting rounds (n=20) and early stopping rounds (n=5) to prevent overfitting and reduce training time. Training will cease if there is no improvement in the performance metrics on the validation dataset for five consecutive rounds. The save_model() function is utilized to save the trained model in a text file for subsequent use.

2.2.4 Model Training

Patients were randomly allocated into a training set (n=150) and a validation set (n=29) for the development and validation of the Light-GBM predictive model. The model was

established based on 17 clinical features, including age, cancer stage, tumor size, tumor location, medical history, chemotherapy, targeted and hormone therapy drugs, distant metastases, surgery, radiation therapy position and dose, ECG signal score, and LVEF value prior to radiotherapy. To mitigate the risk of overfitting due to an excessive maximum tree depth in our small dataset, specific configurations were set as follows: the number of leaves at 31, the learning rate at 0.05, "feature_fraction" at 0.9, and "bagging_fraction" at 0.8.

Lastly, to evaluate the model, a 10-fold cross-validation method is employed to assess its performance and generalization capabilities. This approach helps ensure that the model is not overfitting to a specific training set and can perform well on unseen data. The dataset was divided into ten equal folds, with the training and validation process carried out ten times. In each iteration, nine folds are used for training, while the remaining fold serves as a validation set to assess the model's performance. This process is repeated ten times, with each fold acting as the validation set exactly once. The performance of the model was obtained by averaging all ten AUC values.

2.3 Results

2.3.1 AUC

The ROC curve for our Light-GBM model is shown in Figure6. With an AUC value of 0.82, which is significantly higher than the clinical threshold of 0.7, our model demonstrates strong performance in predicting cardiotoxicity for breast cancer patients undergoing chemoradiotherapy.

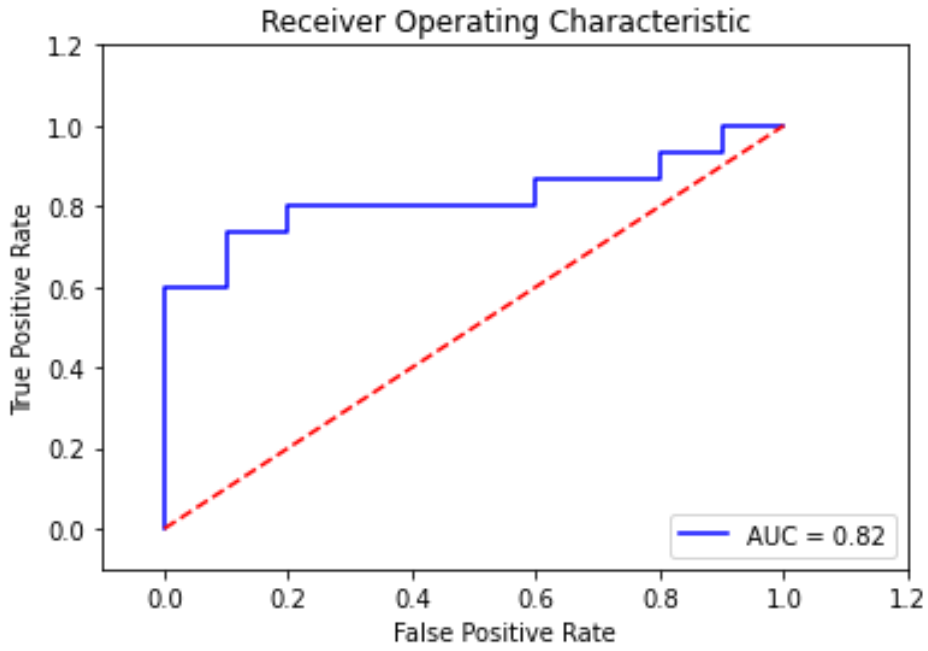

Figure 6: ROC curve of our Light-GBM model. The AUC value is 0.82.

2.3.2 Feature Importance

Our results suggested that the two most severe cardiotoxicity-related features for patients analyzed by the Light-GBM model are patients' age and LVEF value before radiotherapy by “lgb.plot.importance” function. Features with higher importance are more influential in the model's predictions and should be considered more carefully when interpreting the model's output. As shown in Figure 7, these two features scored 105 and 97 in total, indicating greater importance than other features. Cancer position, chosen target therapy drugs, chosen chemotherapy drugs, ECG signal before radiotherapy, and tumor stage also have a significant influence on the model results (22-31 scores).

The results showed that cardiotoxicity increases with older age, later tumor stage, lower LVEF value before radiotherapy, and abnormal ECG signals with bradycardia, tachycardia, T wave, and Q wave abnormalities. Moreover, patients who received epirubicin and doxorubicin as chemotherapy drugs and took bevacizumab and pertuzumab as targeted therapy drugs exhibited more severe cardiotoxicity than others.

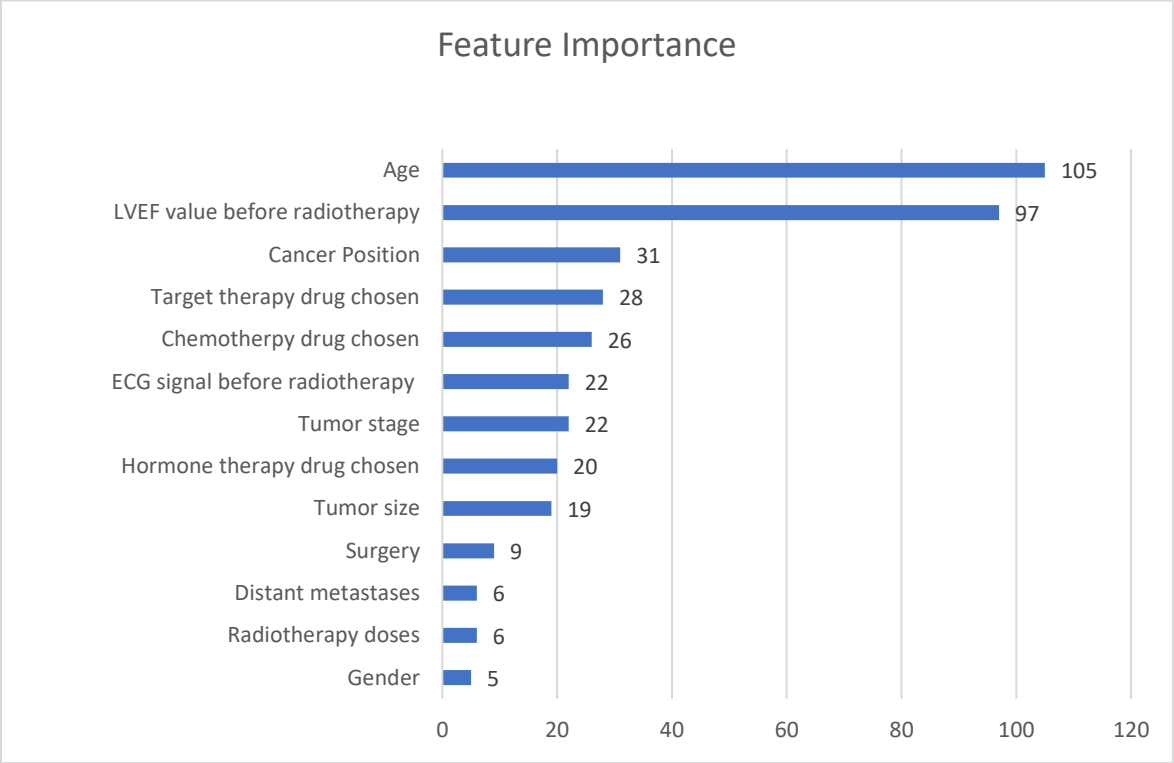

Figure 7: Feature importance distribution by Light-GBM Model predicted, which Age, LVEF value before radiotherapy, cancer position, targeted/chemotherapy therapy drug chosen, and ECG signal are most considered influence factors.

2.4 Statistical Analysis

The performance of the Light-GBM model is summarized in Table 2. For the validation set, the model achieved a sensitivity of 78.6%, specificity of 81.8%, F1 score of 81.5%, precision of 84.6%, and overall accuracy of 80.0%. For statistical analysis, a 10-fold cross-validation was conducted by randomly permuting the target variable from the dataset ten times in both the training set (n=150) and test set (n=29). The average of the ten AUC values is 0.822, with a standard deviation (σ) of 0.069 and a standard error of the mean (SEM) of 0.02.

Table 2. The Performance of Light-GBM Model

	AUC	Sensitivity	Specificity	F1 score	Precision	Accuracy
	0.82 ±0.02	0.79 ±0.03	0.82 ±0.05	0.815 ±0.02	0.846 ±0.02	0.8 ±0.04
Light-GBM Model: using 17 Clinical, Ultrasound and ECG features						

2.5 Discussion

To the best of our knowledge, this is the first study to utilize a Light-GBM to construct predictive models that integrate patients' EMRs to predict cardiotoxicity in patients years after chemoradiotherapy treatment. The results of the performance of the model suggest that the Light-GBM model developed in this study is effective in identifying patients who are at high risk of cardiotoxicity.

The study included 179 patients with stage I-IV breast cancer who underwent both radiation therapy and chemotherapy at Sichuan Cancer Hospital. We found that age, LVEF value

before radiotherapy, cancer position, targeted therapy, tumor stage, and hormone therapy were the most influential factors. Similar research, such as Ryberg et al [38], has previously identified older age, targeted therapy, later tumor stage, hormone therapy, anthracyclines, targeted drugs, and abnormal ECG signals before therapy as risk factors for cardiotoxicity. However, our results suggest that patients with higher LVEF values before radiotherapy experienced more severe cardiotoxicity.

The findings by Potter et al indicated that Radiation therapy-induced changes in the ECG are common among patients with breast cancer. By demonstrating simultaneous correlation with structural and functional changes in echocardiography, ECG changes can serve as surrogate markers for the assessment of the impact of radiation therapy on the heart in this patient population, both during the screening process and in follow-up evaluations [52].

Recent studies have demonstrated that 2D strain analysis has lower or comparable intra- and inter-observer variability than 2D LVEF, and it is more sensitive in detecting changes in left ventricular (LV) function [52, 53]. As a result, in future studies, we could consider utilizing speckle-tracking imaging to detect cardiac function and optimize the predictive power of the model.

The limitation of our study is a small sample set limited by missing DICOM files for some patients due to the long data collection period (2005-2020). In this study, we only used the clinical characteristics as the training data for our Light-GBM Model. We have put the 17 clinical features of 150 patients into the training dataset to train and optimize the model. The AUC value of the Light-GBM predictive model achieved in the validation set was 0.82. A larger sample size with an increased number of features would undoubtedly enhance the predictive capabilities of the model substantially. In future studies, by employing a more extensive sample

size and incorporating additional feature information, the model's predictive ability could be significantly improved. For instance, Jiang et al. achieved impressive results by combining clinical, dosimetric, and radiomics features in their machine learning model for predicting radiation pneumonitis from planning CT images [54]. Furthermore, additional image factors from breast cancer patients' DICOM and CT files will be included in future study, allowing us to determine the influencing factors of cardiotoxicity more accurately [44].

. The developed model allows radiation oncologists and medical physicists to optimize treatment planning and assess whether patients require early clinical intervention. Ultimately, this model could significantly reduce the impact of cardiotoxicity for breast cancer patients undergoing both radiotherapy and chemotherapy.

Chapter 3 Development and validation of a light-GBM enabled model to predict radiation-induced toxicity in nasopharynx cancer patients undergoing radiotherapy

3.1 Introduction

Nasopharyngeal cancer is known to be sensitive to radiation therapy. While radiation therapy effectively destroys tumor cells, it also inevitably exposes normal tissue or organ cells to radiation. Systemic radiation reactions include fatigue, dizziness, decreased appetite, nausea, vomiting, alterations in taste, and sleep disturbances. Mucosal reactions can occur after a radiation dose of 40Gy, causing swelling or congestion in the oral pharynx, nasal pharynx, nasal cavity, and accessory sinuses, and an increase in exudate. In severe cases, this can lead to punctate or patchy membranes [10]. Patients may also experience throat pain, difficulty eating, and nasal congestion during the radiation process.

Other radiation reactions involve the salivary glands, such as decreased saliva secretion, dry mouth, and difficulty swallowing, as well as radiation injury to the brain and spinal cord [55]. Research has linked higher doses in areas such as the floor of the mouth, oral cavity, submandibular glands, parotid glands, brainstem's area postrema, and other sites to more severe toxicities [56-60], Prior studies have investigated radiation toxicity in head and neck tumors, with published reports mainly focusing on oral mucositis, ocular toxicity, thyroid toxicity, pharyngeal toxicity, muscular toxicity, and radiation otitis media which significantly impact the quality of life for patients [61-65]. These studies predominantly emphasized clinical follow-up evaluations of toxicities, lacking quantitative assessment methods. Ishibashi N et al. [62] employed CT values of the thyroid gland before and after radiation to evaluate thyroid radiation toxicity, while Huang X et al. utilized CT values to assess sarcopenia induced by radiotherapy

[64]. Additionally, serum markers such as thyroid function and pretreatment serum vitamin levels have been used in radiation-induced thyroid toxicity and oral mucositis studies [63, 66]. However, these investigations only addressed single toxicities and did not provide a comprehensive quantitative assessment of multiple toxicities.

Moreover, studies predicting radiotherapy toxicity are relatively scarce. Most have explored the correlation between toxicity and radiation dose based on the occurrence of corresponding toxicity, summarizing dose thresholds for specific toxicities. These studies did not employ predictive models. Guo Li et al.[67] used a Cox proportional hazards model, highlighting the detrimental impact of the vicious cycle of acute radiation toxicities and weight loss on NPC patient prognosis. However, due to the absence of established machine learning models, the performance of the AUC value was suboptimal. Machine learning models, which possess superior prediction capabilities, have only been applied to predict breast skin toxicity and radiation pneumonitis [53, 68].

To mitigate the occurrence of various toxicities and enhance patients' quality of life, there is an urgent need for an effective machine learning prediction model that addresses a wide range of radiation toxicities. In this study, we innovatively conduct quantitative assessments and grading of toxicities by comparing CT values, organ cross-sectional diameter/area/width/thickness changes in MRI/CT before and after radiotherapy. For the first time, to the best of our knowledge, we developed a Light-GBM tool for early prediction of severe radiation-induced toxicities. This tool is based on dose distribution, radiomics features within three ROIs, and patient physical information, as well as targeted therapy and chemotherapy regimens.

3.2 Material and Methods

3.2.1 Patients and Inclusion Criteria

A total of 223 patients with nasopharynx cancer receiving RT at Sichuan Cancer hospital, Chengdu, China between 2018 and 2021 were included in this study. All the patients were followed up in two months to two and half years after they received radiation therapy. All patients received pre- and post-RT MRI/CT scans. Toxicity outcomes were determined by comparing pre-RT and post-RT MRI/CT scans. Experienced radiologists assessed changes in CT values, organ section dimensions (diameter, area, and width), and skin thickness.

Patients were categorized as having toxicity or non-toxicity based on the CTCAE (Common Terminology Criteria for Adverse Events) cut-off value of $\geqslant 2$. The CTCAE cut-off value serves as a threshold in clinical research to distinguish between varying degrees of adverse events or toxicities experienced by patients during treatment. Developed by the National Cancer Institute (NCI), this standardized classification system consistently describes and grades the severity of side effects caused by cancer therapies. A CTCAE cut-off value of $\geqslant 2$ encompasses all adverse events classified as grade 2 (moderate) or higher, emphasizing the focus on more severe toxicities.

3.2.2 Features and Feature Normalization

All the patients who have lost most of their data were excluded from this study. For patients who lack one or two features, as “N/A” only precents a small number of total features for each patient (0.56% to 4.47%), we consider “N/A” as the median number of that feature for all patients.

As shown in Table 2, the clinical features used in the study include gender, age, cancer stage, tumor size and location, chemotherapy and targeted therapy drugs, distant metastases, radiation therapy position and dose. Additionally, 756 radiomic features were extracted from images of the gross target volume (GTV), clinical target volume (CTV), CTV-GTV, planning target volume (PTV), and organs at risk (OAR) regions, and were selected as the training features. The IBEX 6.10 software was used to extract those radiomics features from 17 different regions of interest (ROIs) in treatment planning images, organized into 5 feature categories.

To speed up the model training, all the features were normalized within the range of 0 to 1. We represented all "yes or no" questions (heart disease history, distant metastases, hormone therapy, target therapy drugs) into 1 and 0, with patients having none of these conditions as 0, and opposite as 1. For gender (male or female) and cancer position (left or right) those only have two sides features, we unified male, left as 0, and female, right as 1. We divided age and dose values by 100. For cancer stage, we set stage 1 as 0, stage 2 as 0.33, stage 3 as 0.66 and stage 4 as 1. For chemotherapy drugs and target therapy drugs, we consider arrhythmia, premature atria, and premature ventricular beats, we set them as 0.1. Bradycardia and tachycardia as 0.2. And according to different chemotherapy drugs and target therapy drugs' potential toxicity influence, we consider Epicorubicin and doxorubicin as 0.3. Cyclophosphamide, paclitaxel, and docetaxel as 0.2. Capecitabine, vinorelbine, gemcitabine, cisplatin, nedaplatin, carboplatin, xeloda as 0.3. Same with target therapy drugs, we set Bevacizumab as 0.3, Pertuzumab as 0.2 and Pertuzumab as 0.1. All optimized feature values are consolidated in Excel files to facilitate seamless integration with the Light-GBM model.

Table3: Training Clinical factors for Light-GBM Model

Variable		Number	Percentage
Gender	Male	138	61.88%
	Female	85	38.12%
Age	<44	69	30.08%
	44~62	94	42.15%
	>62	60	26.90%
Tumor size	T1	36	16.14%
	T2	67	30.04%
	T3	64	28.69%
	T4	56	25.11%
Cancer position	Left	78	34.98%
	Middle	65	29.15%
	Left	80	35.87%
Cancer stage	I	14	6.28%
	II	69	30.94%
	III	40	17.94%
	IV	100	44.84%
Distant metastases	Yes	192	86.09%
	No	31	13.90%
chemotherapy drugs	Epicorubicin and doxorubicin	167	74.89%
	Cyclophosphamide, paclitaxel, and docetaxel	46	20.63%
	Capecitabine, vinorelbine, gemcitabine,	3	1.35%
	cisplatin, nedaplatin, carboplatin, xeloda	4	1.79%
radiotherapy dose	<65Gy	27	1.21%
	65~70GY	160	71.75%
	>70GY	36	16.14%
targeted therapy	Yes	144	64.57%
	No	79	35.42%
targeted therapy drugs	Trastuzumab	163	73.09%
	Pertuzumab	50	22.42%
	Bevacizumab	10	4.48%

3.2.3 Light-GBM Model Building and Training

The Light-GBM model and Python program were employed in this study. In the study of nasopharynx cancer patients, 223 patients were randomly divided into a training set of 203 patients and a validation set of 20 patients. The Light-GBM model was developed using only clinical features (Model A) or a combination of clinical and radiomic features (Model B). The performance of the models in predicting severe toxicities was evaluated using ROC analysis on the validation cohort.

3.3 Results

3.3.1 AUC

We developed two distinct models for more effective comparison of results. Model A, which incorporates only clinical features, yielded AUC values for sternocleidomastoid muscle toxicity, radiation oral mucositis, radiation dermatitis, skin ulcer, thyrotoxicity, and skin thickness toxicities of 0.8, 0.71, 0.72, 0.68, 0.75, and 0.64, respectively (Figure 8). Upon incorporating radiomics features into the Light-GBM model training for Model B, the AUC values for the six toxicities improved to 0.86, 0.81, 0.84, 0.77, 0.89, and 0.8 (Figure 9). The results demonstrated that by incorporating radiomic features, the accuracy of the Light-GBM model has significantly improved.

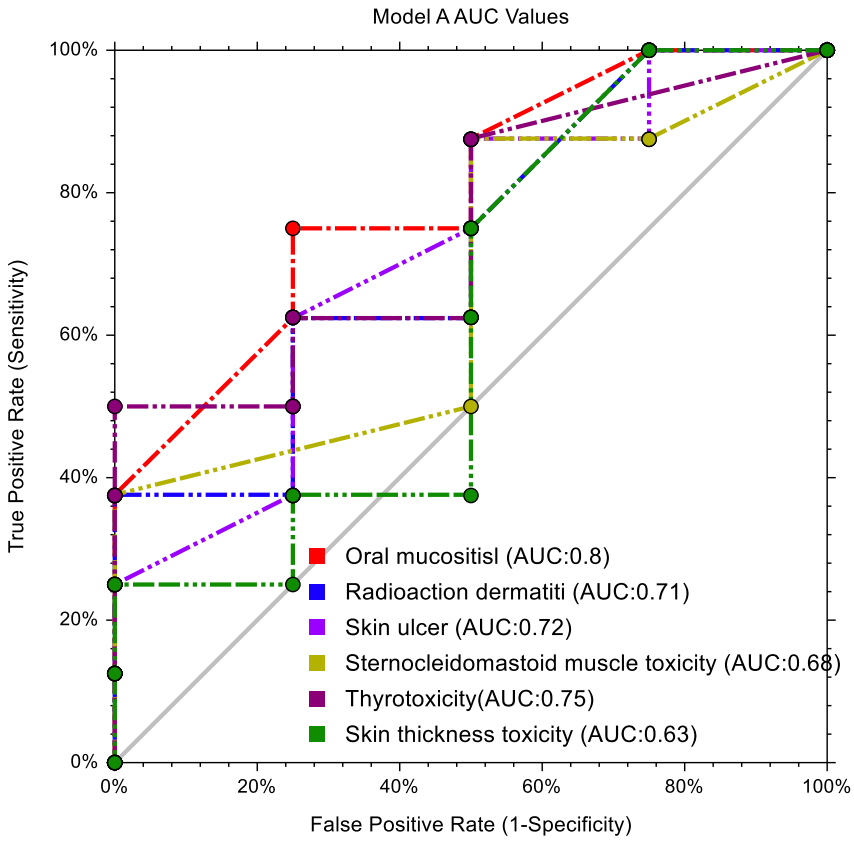

Figure 8: The receiver operating characteristic (ROC) curves for Model A, which only built with clinical factors.

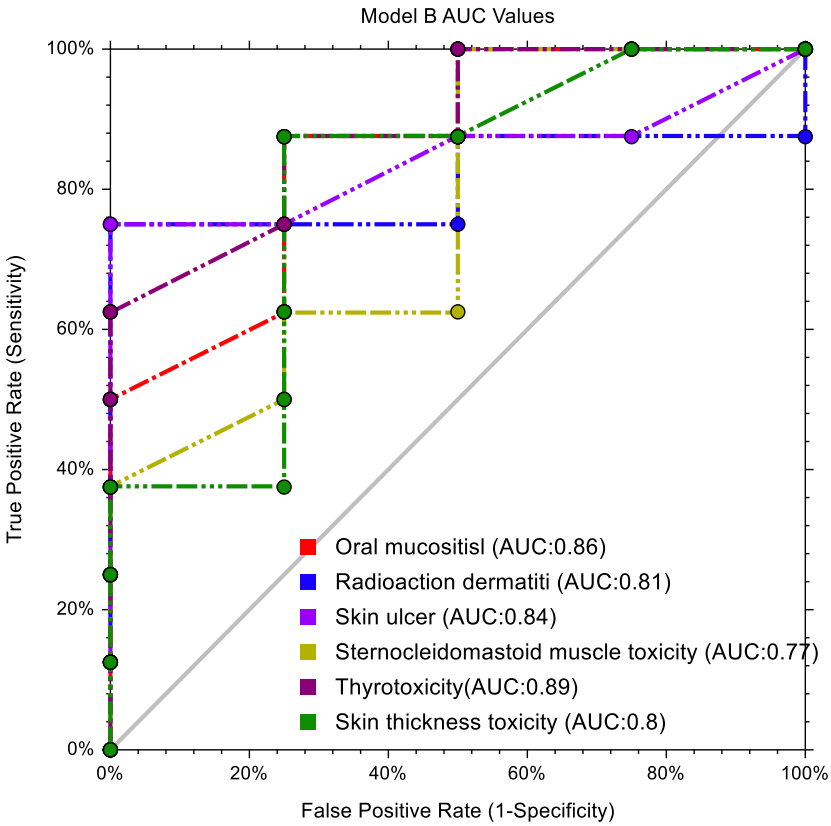

Figure 9: The ROC curves for Model B, which training by combining clinical and dosimetry factors.

3.3.2 Feature Importance

In this study, we also employed the "lgb.plot_importance" function from the Light-GBM library in Python to examine the significance of features for model prediction. The feature importance analysis revealed that T stage, age, radiation dose, chemotherapy drugs, and 14 distinct radiomic features were the most valuable risk prediction factors, as shown in Figure 10. Later T stages, older age, higher radiation doses, and increased PTV, CTV, and GTV values were associated with more severe toxicity than others.

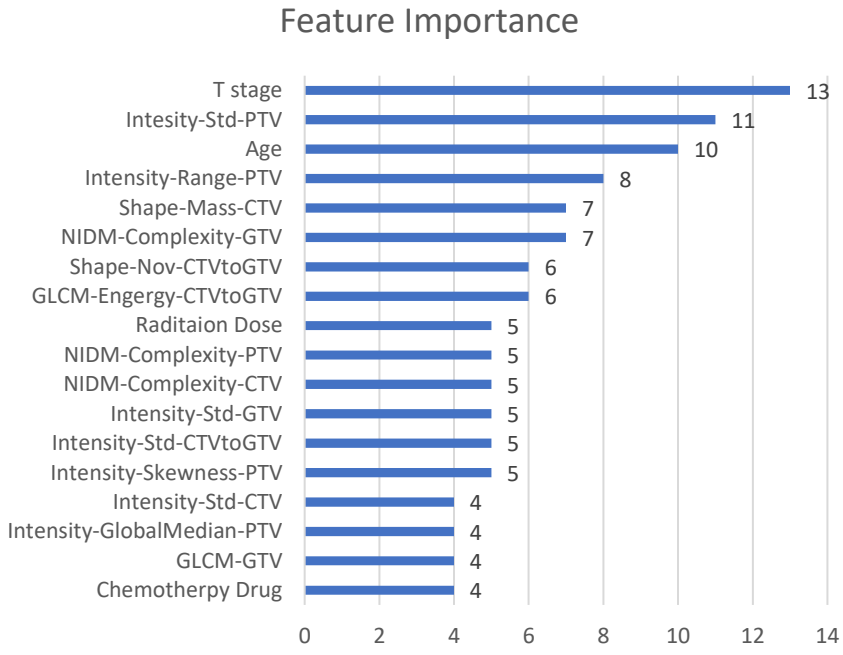

Figure 10: Total feature importance analysis to show the most valuable influencing factors that contributes to the prediction of Light-GBM Models. Abbreviations: Std =Standard; NIDM =neighborhood intensity difference matrix; Nov =Number of Voxel; GLCM =gray-level co-occurrence matrix

3.4 Statistical Analysis

The calculated t-value between the two distinct models, at 6.82, considerably surpasses the critical t-value of 2.571. As a result, the null hypothesis can be rejected, denoting a statistically significant difference between the two models. The combined Model B outperforms Model A, which was dependent solely on clinical features.

3.5 Discussion

NPC is known to be sensitive to radiation therapy, which serves as the preferred treatment method for this type of cancer [69]. However, due to the inevitable exposure of surrounding healthy tissue to radiation, NPC patients may experience complications such as oral mucositis, radiation dermatitis, skin ulceration, changes in sternocleidomastoid muscle thickness, and thyroid toxicity after radiation therapy [61, 68, 70]. These complications can lead to pain, difficulty swallowing, weight loss, and may even necessitate treatment cessation, resulting in delayed tumor treatment and a reduced quality of life. Predicting radiation toxicity effectively can help identify patients at risk of developing severe radiation toxicity following chemotherapy, providing a basis for adjusting clinical treatment plans, reducing toxicity occurrences, and ensuring treatment completion.

To enhance the prediction of radiotherapy toxicity in nasopharyngeal cancer patients, we developed a Light-GBM model based on clinical features and radiomics features for the first time. The challenge in controlling post-radiotherapy toxicity lies in optimizing the radiotherapy dose distribution to minimize late toxicity. For example, Xiao et al [71] demonstrated that employing IMRT and SMART (simultaneous modulated accelerated radiation therapy) can protect healthy tissue, reduce late toxicity through optimal dose distribution, and improve long-term local control rates when combined with synchronous chemotherapy.

In this study, we assessed toxicity by comparing changes in CT values, organ cross-sectional dimensions (diameter, area, and width), and skin thickness between pre-radiotherapy MRI/CT and post-radiotherapy MRI/CT scans, as evaluated by experienced radiation oncologists. Out of the 223 patients included in this study, 71 patients (31% ratio) with a

CTCAE ≥ 2 were determined to have radiotherapy toxicity, which is consistent with previous studies.

We have developed two distinct Light GBM models to predict radiation-induced toxicity in nasopharyngeal cancer patients by incorporating clinical variables and/or radiomic features. Model A includes only clinical features, while Model B optimizes the model by adding radiotherapy parameters, which significantly improves the AUC value compared to previous studies [72]. Effectively predicting radiotherapy toxicity helps identify nasopharyngeal cancer patients at risk of severe radiation toxicity after chemotherapy. This enables adjustments to clinical treatment plans, reduces the occurrence of toxicities, ensures treatment completion as planned, and improves patient quality of life post-tumor cure.

Feature importance analysis reveals that T stage, age, radiation dose, chemotherapy drugs, and 14 radiomic features are the most valuable risk prediction factors. Patients with a late T stage, older age, higher radiation dose, and higher PTV, CTV, and GTV values of drugs exhibit more severe toxicity than others. To the best of our knowledge, our AUC results are comparable to or even surpass some related studies, such as the prediction of radiotherapy-induced xerostomia in head and neck squamous cell carcinoma, as seen in the RTOG 0522 clinical trial [72]. Table 3 shows a comparison of some of our results with other people's work.

Table 4: Comparison of some model prediction results with other work.

Method	Toxicity Type	AUC Values
Men's 3D rCNN[70]	Xerostomia	0.82
Men's 3D rCNN without CT[70]	Xerostomia	0.78
Light-GBM Model	Radiation Oral Mucositis	0.86
Light-GBM Model	Radiation Dermatitis	0.81

In contrast to previous studies that focused on specific radiotherapy-induced toxicities, our research comprehensively investigates radiation-induced oral mucositis, radiation dermatitis, skin ulcers, chest wall pectoral muscle toxicity, thyroid toxicity, and skin thickness toxicity. We adopted the CTCAE $\geqslant$ 2 standard, as in prior studies [73], for assessing toxicity. Additionally, we involved experienced radiation oncologists in the evaluation of pre- and post-radiotherapy imaging, an innovative approach that enables more accurate toxicity determinations.

Nonetheless, our study has limitations, being a single-center retrospective study. Future research could expand the sample size and conduct multi-center or prospective studies to acquire more reliable clinical data. This would enhance the model's predictive performance and better aid radiation oncologists in proactively preventing toxicity, adjusting radiotherapy plans promptly, and ultimately improving patients' quality of life.

Despite its limitations, our study delivers valuable insights into predicting radiation-induced toxicity in nasopharyngeal cancer patients. By combining clinical variables and radiomic features, our models contribute to a better understanding of factors influencing toxicity risk. This

knowledge can potentially inform clinical decision-making, facilitating more personalized treatment plans that minimize severe toxicity risks while maximizing therapeutic outcomes.

Chapter 4 Conclusion

To summarize, our study demonstrated that the Light-GBM classifier can be utilized to develop predictive models for radiotherapy-induced breast cancer and nasopharynx cancer toxicity, which can automatically predict different toxicities using EMR data and patients' images. We successfully established an early toxicity risk prediction model that can facilitate the identification of cancer patients who are likely to develop severe radiation-induced toxicities after chemoradiotherapy.

The ability to identify patients with potential cardiotoxicity and nasopharynx toxicity early on using an inexpensive and widely available point-of-care test has significant practical implications for toxicity diagnosis and management of patients from a precision medicine perspective. Our research has the potential to enhance the effectiveness of cancer treatments and improve patient outcomes.

References

1. Bentzen, S.M., *Preventing or reducing late side effects of radiation therapy: radiobiology meets molecular pathology.* Nature Reviews Cancer, 2006. **6**(9): p. 702-713.
2. Royce, T.J., M.M. Qureshi, and M.T. Truong, *Radiotherapy utilization and fractionation patterns during the first course of cancer treatment in the United States from 2004 to 2014.* Journal of the American College of Radiology, 2018. **15**(11): p. 1558-1564.
3. De Ruysscher, D., et al., *Radiotherapy toxicity.* Nature Reviews Disease Primers, 2019. **5**(1): p. 1-20.
4. Marks, L.B., et al., *Use of normal tissue complication probability models in the clinic.* International Journal of Radiation Oncology* Biology* Physics, 2010. **76**(3): p. S10-S19.
5. Baskar, R., et al., *Cancer and radiation therapy: current advances and future directions.* International journal of medical sciences, 2012. **9**(3): p. 193.
6. Delaney, G., et al., *The role of radiotherapy in cancer treatment: estimating optimal utilization from a review of evidence-based clinical guidelines.* Cancer: Interdisciplinary International Journal of the American Cancer Society, 2005. **104**(6): p. 1129-1137.
7. DeSantis, C.E., et al., *Breast cancer statistics, 2019.* CA: a cancer journal for clinicians, 2019. **69**(6): p. 438-451.
8. Duane, F.K., et al., *Cardiac structure doses in women irradiated for breast cancer in the past and their use in epidemiological studies.* Practical radiation oncology, 2019. **9**(3): p. 158-171.
9. McDonald, M.W., et al., *Acute toxicity in comprehensive head and neck radiation for nasopharynx and paranasal sinus cancers: cohort comparison of 3D conformal proton*

therapy and intensity modulated radiation therapy. Radiation oncology, 2016. **11**(1): p. 1-10.

10. Lee, A.W., et al., *Evolution of treatment for nasopharyngeal cancer–success and setback in the intensity-modulated radiotherapy era.* Radiotherapy and Oncology, 2014. **110**(3): p. 377-384.
11. Law, M.Y. and B. Liu, *DICOM-RT and its utilization in radiation therapy.* Radiographics, 2009. **29**(3): p. 655-667.
12. Ger, R.B., et al., *Guidelines and experience using Imaging Biomarker Explorer (IBEX) for radiomics.* JoVE (Journal of Visualized Experiments), 2018(131): p. e57132.
13. Zhang, L., et al., *IBEX: an open infrastructure software platform to facilitate collaborative work in radiomics.* Medical physics, 2015. **42**(3): p. 1341-1353.
14. Haralick, R.M., K. Shanmugam, and I.H. Dinstein, *Textural features for image classification.* IEEE Transactions on systems, man, and cybernetics, 1973(6): p. 610-621.
15. Galloway, M.M., *Texture analysis using gray level run lengths.* Computer graphics and image processing, 1975. **4**(2): p. 172-179.
16. Tang, X., *Texture information in run-length matrices.* IEEE transactions on image processing, 1998. **7**(11): p. 1602-1609.
17. Zhou, W., et al., *Application of LightGBM algorithm to classification of structural magnetic resonance imaging in Alzheimer's disease.* Chin. J. Med. Phys., 2019. **36**(4): p. 408-413.
18. Zhang, D. and Y. Gong, *The comparison of LightGBM and XGBoost coupling factor analysis and prediagnosis of acute liver failure.* IEEE Access, 2020. **8**: p. 220990-221003.

19. Ke, G., et al., *Lightgbm: A highly efficient gradient boosting decision tree.* Advances in neural information processing systems, 2017. **30**.

20. Ling, D.C., et al., *Incidence of hospitalization in patients with head and neck cancer treated with intensity-modulated radiation therapy.* Head & neck, 2015. **37**(12): p. 1750-1755.

21. Ranka, S. and V. Singh. *CLOUDS: A decision tree classifier for large datasets*. in *Proceedings of the 4th knowledge discovery and data mining conference*. 1998.

22. Fisher, W.D., *On grouping for maximum homogeneity.* Journal of the American statistical Association, 1958. **53**(284): p. 789-798.

23. Gao, W., et al., *Prediction of acute kidney injury in ICU with gradient boosting decision tree algorithms.* Computers in Biology and Medicine, 2022. **140**: p. 105097.

24. Lasko, T.A., et al., *The use of receiver operating characteristic curves in biomedical informatics.* Journal of biomedical informatics, 2005. **38**(5): p. 404-415.

25. Shapiro, D.E., *The interpretation of diagnostic tests.* Statistical methods in medical research, 1999. **8**(2): p. 113-134.

26. Zweig, M.H. and G. Campbell, *Receiver-operating characteristic (ROC) plots: a fundamental evaluation tool in clinical medicine.* Clinical chemistry, 1993. **39**(4): p. 561-577.

27. Mamoshina, P., B. Rodriguez, and A. Bueno-Orovio, *Toward a broader view of mechanisms of drug cardiotoxicity.* Cell Reports Medicine, 2021. **2**(3): p. 100216.

28. Group, E.B.C.T.C., *Effects of radiotherapy and of differences in the extent of surgery for early breast cancer on local recurrence and 15-year survival: an overview of the randomised trials.* The Lancet, 2005. **366**(9503): p. 2087-2106.

29. Darby, S.C., et al., *Risk of ischemic heart disease in women after radiotherapy for breast cancer*. New England Journal of Medicine, 2013. **368**(11): p. 987-998.

30. Giordano, S.H., et al., *Risk of cardiac death after adjuvant radiotherapy for breast cancer*. Journal of the National Cancer Institute, 2005. **97**(6): p. 419-424.

31. Darby, S.C., et al., *Long-term mortality from heart disease and lung cancer after radiotherapy for early breast cancer: prospective cohort study of about 300 000 women in US SEER cancer registries.* The lancet oncology, 2005. **6**(8): p. 557-565.

32. Litt, H. and W. Hwang, *Coronary artery findings after left-sided compared with right-sided radiation treatment for early-stage breast cancer*. J Clin Oncol, 2007. **25**: p. 3031-7.

33. Wang, W., et al., *Quantitative coronary angiography findings of patients who received previous breast radiotherapy.* Radiotherapy and Oncology, 2011. **100**(2): p. 184-188.

34. Nilsson, G., et al., *Distribution of coronary artery stenosis after radiation for breast cancer*. Journal of clinical oncology, 2012. **30**(4): p. 380-386.

35. Zagar, T.M. and L.B. Marks, *Breast cancer radiotherapy and coronary artery stenosis: location, location, location.* Journal of clinical oncology: official journal of the American Society of Clinical Oncology, 2011. **30**(4): p. 350-352.

36. Kosaraju, A., et al., *Left ventricular ejection fraction.* 2017.

37. Gkantaifi, A., et al., *Breast radiotherapy and early adverse cardiac effects. The role of serum biomarkers and strain echocardiography.* Anticancer Research, 2019. **39**(4): p. 1667-1673.

38. Ryberg, M., et al., *New insight into epirubicin cardiac toxicity: competing risks analysis of 1097 breast cancer patients.* Journal of the National Cancer Institute, 2008. **100**(15): p. 1058-1067.

39. Mele, D., et al., *Cancer therapy-induced cardiotoxicity: role of ultrasound deformation imaging as an aid to early diagnosis.* Ultrasound in medicine & biology, 2015. **41**(3): p. 627-643.

40. Liu, J., et al., *Contemporary role of echocardiography for clinical decision making in patients during and after cancer therapy.* JACC: Cardiovascular Imaging, 2018. **11**(8): p. 1122-1131.

41. Perez, I.E., et al., *Cancer therapy-related cardiac dysfunction: an overview for the clinician.* Clinical Medicine Insights: Cardiology, 2019. **13**: p. 1179546819866445.

42. Anthony, F.Y., et al., *Assessment of early radiation-induced changes in left ventricular function by myocardial strain imaging after breast radiation therapy.* Journal of the American Society of Echocardiography, 2019. **32**(4): p. 521-528.

43. Schofield, R., et al. *Textural analysis: Virtual histological examination of the left ventricular myocardium using SSFP cines in CMR: Extracting more detail than the human eye can perceive*. in *EUROPEAN HEART JOURNAL*. 2016. OXFORD UNIV PRESS GREAT CLARENDON ST, OXFORD OX2 6DP, ENGLAND.

44. Löffler, A.I. and M. Salerno, *Cardiac MRI for the evaluation of oncologic cardiotoxicity.* Journal of Nuclear Cardiology, 2018. **25**(6): p. 2148-2158.

45. Chang, W.-T., et al., *An artificial intelligence approach for predicting cardiotoxicity in breast cancer patients receiving anthracycline.* Archives of Toxicology, 2022. **96**(10): p. 2731-2737.

46. Grela-Wojewoda, A., et al., *Biomarkers of Trastuzumab-Induced Cardiac Toxicity in HER2-Positive Breast Cancer Patient Population.* Cancers, 2022. **14**(14): p. 3353.

47. Piveta, R.B., et al., *Early change in area strain detected by 3D speckle tracking is associated with subsequent cardiotoxicity in patients treated with low doses of anthracyclines.* Frontiers in Cardiovascular Medicine, 2022. **9**: p. 842532.

48. Gu, J., et al., *Assessment of Global Cardiac Function Using AutoSTRAIN Automatic Strain Quantitative Technology in Patients With Breast Cancer Undergoing Anthracycline-Based Chemotherapy.* Ultrasound in Medicine & Biology, 2023. **49**(1): p. 368-374.

49. Park, H., et al., *Left atrial longitudinal strain as a predictor of Cancer therapeutics-related cardiac dysfunction in patients with breast Cancer.* Cardiovascular Ultrasound, 2020. **18**: p. 1-8.

50. Bobrowski, D., et al., *The yield of routine cardiac imaging in breast cancer patients receiving trastuzumab-based treatment: a retrospective cohort study.* Canadian Journal of Cardiology, 2020. **36**(10): p. 1658-1666.

51. Tuohinen, S.S., et al., *Radiotherapy-induced early ECG changes and their comparison with echocardiography in patients with early-stage breast cancer.* Anticancer Research, 2018. **38**(4): p. 2207-2215.

52. Potter, E. and T.H. Marwick, *Assessment of left ventricular function by echocardiography: the case for routinely adding global longitudinal strain to ejection fraction.* JACC: Cardiovascular Imaging, 2018. **11**(2 Part 1): p. 260-274.

53. Jiang, W., et al., *Dosimetric factors and radiomics features within different regions of interest in planning CT images for improving the prediction of radiation pneumonitis.*

International Journal of Radiation Oncology* Biology* Physics, 2021. **110**(4): p. 1161-1170.

54. Wehner, G.J., et al., *Routinely reported ejection fraction and mortality in clinical practice: where does the nadir of risk lie?* European heart journal, 2020. **41**(12): p. 1249-1257.

55. Sun, X., et al., *Long-term outcomes of intensity-modulated radiotherapy for 868 patients with nasopharyngeal carcinoma: an analysis of survival and treatment toxicities.* Radiotherapy and oncology, 2014. **110**(3): p. 398-403.

56. Kumar, R., et al., *Radiation dose to the floor of mouth muscles predicts swallowing complications following chemoradiation in oropharyngeal squamous cell carcinoma.* Oral oncology, 2014. **50**(1): p. 65-70.

57. Bhide, S.A., et al., *Dose–response analysis of acute oral mucositis and pharyngeal dysphagia in patients receiving induction chemotherapy followed by concomitant chemo-IMRT for head and neck cancer.* Radiotherapy and Oncology, 2012. **103**(1): p. 88-91.

58. Eisbruch, A., et al., *Chemo-IMRT of oropharyngeal cancer aiming to reduce dysphagia: swallowing organs late complication probabilities and dosimetric correlates.* International Journal of Radiation Oncology* Biology* Physics, 2011. **81**(3): p. e93-e99.

59. Dirix, P. and S. Nuyts, *Evidence-based organ-sparing radiotherapy in head and neck cancer.* The lancet oncology, 2010. **11**(1): p. 85-91.

60. Kocak-Uzel, E., et al., *Beam path toxicity in candidate organs-at-risk: assessment of radiation emetogenesis for patients receiving head and neck intensity modulated radiotherapy.* Radiotherapy and Oncology, 2014. **111**(2): p. 281-288.

61. Su, C.K., et al., *Phase II double-blind randomized study comparing oral aloe vera versus placebo to prevent radiation-related mucositis in patients with head-and-neck neoplasms.* International Journal of Radiation Oncology* Biology* Physics, 2004. **60**(1): p. 171-177.

62. Ishibashi, N., et al., *Computed tomography density change in the thyroid gland before and after radiation therapy.* Anticancer research, 2018. **38**(1): p. 417-421.

63. Na, G., et al., *Assessment of radiation-induced otitis media in patients with parotid gland malignancy.* Acta Oto-Laryngologica, 2021. **141**(5): p. 466-470.

64. De Bree, R., et al., *Measurement of sarcopenia in head and neck cancer patients and its association with frailty*. Frontiers in Oncology, 2022. **12**.

65. Huang, X., et al., *Severe muscle loss during radical chemoradiotherapy for non-metastatic nasopharyngeal carcinoma predicts poor survival.* Cancer medicine, 2019. **8**(15): p. 6604-6613.

66. Chen, Y.-P., et al., *Nasopharyngeal carcinoma.* The Lancet, 2019. **394**(10192): p. 64-80.

67. Li, G., et al., *Vicious circle of acute radiation toxicities and weight loss predicts poor prognosis for nasopharyngeal carcinoma patients receiving intensity modulated radiotherapy.* Journal of Cancer, 2017. **8**(5): p. 832.

68. Saednia, K., et al., *Quantitative thermal imaging biomarkers to detect acute skin toxicity from breast radiation therapy using supervised machine learning.* International Journal of Radiation Oncology* Biology* Physics, 2020. **106**(5): p. 1071-1083.

69. Tang, L.-L., et al., *Elective upper-neck versus whole-neck irradiation of the uninvolved neck in patients with nasopharyngeal carcinoma: an open-label, non-inferiority, multicentre, randomised phase 3 trial.* The Lancet Oncology, 2022. **23**(4): p. 479-490.

70. Akagunduz, O.O., et al., *Radiation-Induced Ocular Surface Disorders and Retinopathy: Ocular Structures and Radiation Dose-Volume Effect.* Cancer Research and Treatment: Official Journal of Korean Cancer Association, 2022. **54**(2): p. 417.

71. Huang, C.L., et al., *Thyroid dose-volume thresholds for the risk of radiation-related hypothyroidism in nasopharyngeal carcinoma treated with intensity-modulated radiotherapy—A single-institution study.* Cancer medicine, 2019. **8**(16): p. 6887-6893.

72. Men, K., et al., *A deep learning model for predicting xerostomia due to radiation therapy for head and neck squamous cell carcinoma in the RTOG 0522 clinical trial.* International Journal of Radiation Oncology* Biology* Physics, 2019. **105**(2): p. 440-447.

73. Méry, B., et al., *Correlation between anthropometric parameters and acute skin toxicity in breast cancer radiotherapy patients: a pilot assessment study.* The British Journal of Radiology, 2015. **88**(1055): p. 20150414.

Curriculum Vitae

Zirui Jiang, MS

zirui.jiang@unlv.edu, ziruijiang1997@gmail.com

Educational Background

University of Nevada, Las Vegas – M.S. Health Physics (Sub-plan: Medical Physics)

August 2020 – Spring 2023

University of Wisconsin Madison – B.S. Electrical Engineering (Minor: Physics)

August 2015 – Dec 2019

Work and Research Experience

Graduate Assistant – University of Nevada, Las Vegas; Las Vegas, NV

August 2020 – Now

Teaching Assistant

Research Assistant – under Dr. Yu Kuang

Research Assistant – Department of Radiation Oncology, Washington University in St. Louis, St. Louis, MO

February 2020 – August 2020

Work on research projects under the supervision of Prof. Bin Cai

Internship – Department of Radiation Oncology, UT Southwestern Medical Center, Dallas, TX

May 2018 – July 2018

Used a clinical automatic contouring software for abdominal cancer patient

Performed electron beam Monte-Carlo simulations for some patient cases

Used MATLAB to analyze clinical data

Internship – Department of Radiation Oncology, Taipei Medical University Hospital, Taipei

July 2017 – August 2017

Studied the correlation between uterine cancer and the density of muscle

Internship – Marketing Department, Elekta (Beijing) Medical Systems Co., Ltd., Beijing, China

May 2017 – June 2017

Assisted training courses for Elekta linear accelerators and MOSAIQ system

Research Assistant – Department of Radiotherapy, Sichuan Cancer Hospital, Chengdu, China

August 2016, January 2017, August 2018

Conducted literature review on papers related to thyroid and breast ultrasonic diagnosis, and Celiac Plexus Neurolysis

Collected data for three projects

Observed clinical ultrasound diagnosis procedures under attending physician's supervision/

Publications

1. Ziyue Hu, Xueqing Cheng, Juan Li, Jingzhen Jiang, Zirui Jiang, Hui Li, Tingting Li, Zhenqi Zhang, Bo Tan, Man Lu. Preliminary Study of Real-Time Three-Dimensional Contrast Enhanced

Ultrasound of Sentinel Lymph Nodes in Breast Cancer. European Radiology. Accepted

2. Lu Wang, Man Lu, Xiaobo Wu, Xueqing Cheng, Tingting Li, Zirui Jiang, Yuping Shen, Ting Liu,

Yue Ma, Contrast-Enhanced Ultrasound Guided Celiac PlexusNeurolysis in Patients with Upper

Abdominal Cancer Pain: Initial Experience, European Radiology, under revision

3. Tingting Li, Man Lu, Zirui Jiang, Minggang Wu, Ting Wei, Lu Wang, Yanjie Li, Juan Li, Ziyue Hu,

Xueqing Cheng, Computer-aided Diagnosis System of Thyroid Nodules Ultrasonography:

Diagnostic Performance Difference Between CAD and 111 Physicians, Plos One,submitted

4. Juan Li, Lu Wang, Ting Wei, Zirui Jiang, Minggang Wu, Tingting Li, Ziyue Hu, Xueqing Cheng,

Jifen Liao, Zhenqi Zhang, Bo Tan, Man Lu, The concordance in lesion detection and

characteristics between the AI and conventional breast ultrasound Scan method, The breast

Journal